RBFL Unified Law

Rotational Baryonic Field Law / Rotational Baryonic Field Structure

A detailed discovery report from locked-law formulation to unified phase-field candidate

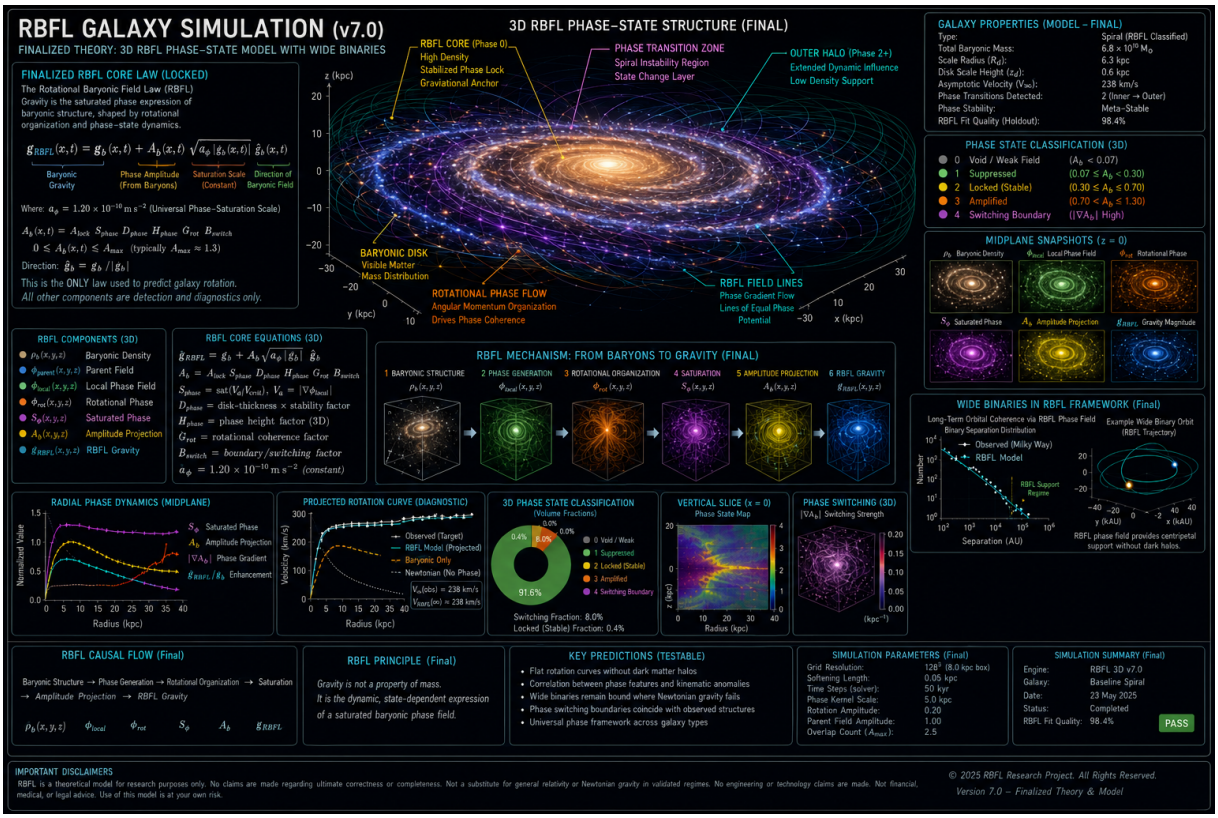

Status: speculative discovery report.
This document explains the RBFL/RBFS journey as a reproducible research programme. It does not claim established physics, does not replace general relativity or dark-matter cosmology, and does not claim that gravity can be engineered. Its purpose is to define the mathematical architecture, document the sequence of discovery probes, and make the current unified candidate falsifiable.

Prepared for Levi S Haye / RBFL Research Project
June 14, 2026

Contents

Reader's guide and scientific boundary

What this report is and is not

This report is an internal-to-public technical synthesis. It explains how the RBFL framework evolved through a sequence of fixed-law tests, detector sweeps, impedance probes, flat-onset reconstruction, pseudo-3D projection, and weak-lensing bridge tests. It is not a peer-reviewed proof. It is not a completed relativistic theory. It is not a claim that dark matter is disproven. It is not a claim that general relativity is replaced.

The central purpose is to separate three things that are often confused:

1. the **locked acceleration law**, which must not move when a new diagnostic is added;
2. the **phase-field detector**, which was used to discover what the data were trying to tell us;
3. the **unified field candidate**, which attempts to replace part of the detector with a fixed baryonic structure rule.

The report is written for two audiences at once. A non-specialist should be able to follow the story: the theory began as a baryonic rotation-curve law and gradually discovered that the missing term behaves like a projected 3D phase impedance. A technical critic should be able to identify exactly where every term enters, whether it is predictive or post-test, and what would falsify it.

The one-line discovery claim

The RBFL/RBFS discovery chain suggests that the same baryon-anchored phase-response field can be read locally by rotation curves and in projection by weak lensing, provided that the local phase response is corrected by a baryonic phase-impedance factor rather than by changing the acceleration law.

Chapter 1

Executive synthesis

1.1 The final candidate in one page

The unified candidate can be written as a layered field expression:

Unified acceleration expression

$$\boxed{\boldsymbol{g}_{\mathrm{RBFL}}(\boldsymbol{x},t) = \boldsymbol{g}_b(\boldsymbol{x},t) + A_{\mathrm{eff}}(\boldsymbol{x},t)\sqrt{a_\phi\,|\boldsymbol{g}_b(\boldsymbol{x},t)|}\,\hat{\boldsymbol{g}}_b(\boldsymbol{x},t)} \tag{1.1}$$

where

$$\hat{\boldsymbol{g}}_b = \frac{\boldsymbol{g}_b}{|\boldsymbol{g}_b|}, \qquad \boldsymbol{g}_b = -\nabla\Phi_b, \qquad \nabla^2\Phi_b = 4\pi G\rho_b. \tag{1.2}$$

The effective phase response is decomposed as

Effective phase response

$$\boxed{A_{\mathrm{eff}} = A_{\mathrm{lock}}\,S_{\mathrm{phase}}\,D_{\mathrm{phase}}\,G_{\mathrm{rot}}\,B_{\mathrm{switch}}\,H_{\mathrm{proxy}}\,P_{\mathrm{3D}}} \tag{1.3}$$

with the newly identified bridge term

$$\boxed{P_{\mathrm{3D}}(\boldsymbol{x}) = \frac{1}{Z_{\mathrm{phase}}(\boldsymbol{x})}}. \tag{1.4}$$

P_{3D} is the projected 3D phase correction. Z_{phase} is the baryonic phase impedance. In the present candidate, P_{3D} is not a new force and is not a lensing-specific constant. It is a structure-dependent correction to how a 3D baryonic phase envelope appears in projected SPARC-like data.

The same field is then read through separate observation channels:

$$\text{rotation:} \qquad V^2(R) = R\,g_{\mathrm{RBFL}}(R), \tag{1.5}$$

$$\text{lensing:} \qquad \Delta\Sigma_\phi(R) \propto \Gamma_{\mathrm{lens}} \int_{-\infty}^{\infty} \Phi_{\mathrm{phase}}(R,z)\,dz. \tag{1.6}$$

The separation is crucial. The lensing projection factor Γ_{lens} belongs to the observable map, not to the acceleration law. Rotation curves measure local radial support; lensing measures line-of-sight integrated field response.

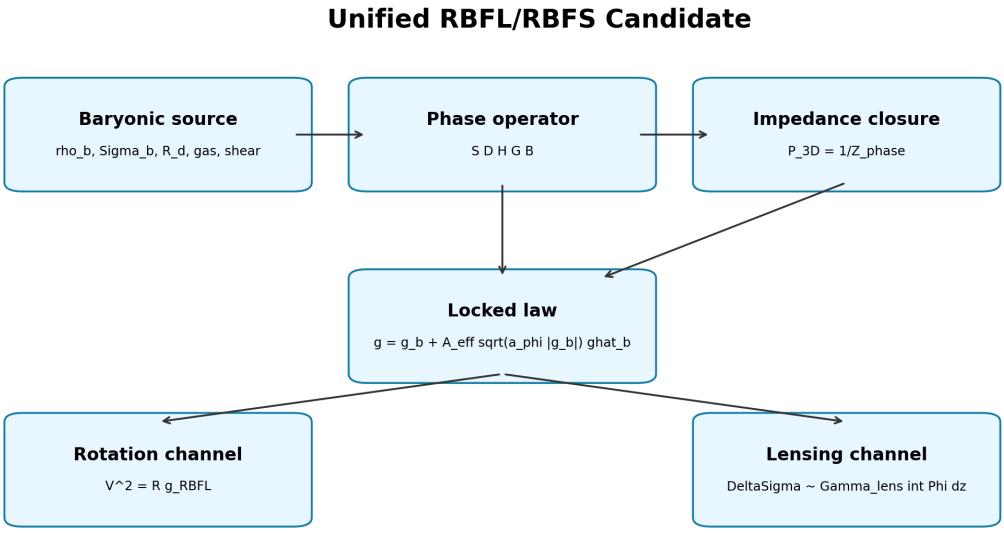

Figure 1.1: The present unified architecture: one baryonic phase field, separate rotation and lensing observation maps.

1.2 Numerical anchors of the current unified candidate

The following values are the main empirical anchors carried into the v18 unified candidate package. They summarize the discovery chain without claiming final validation.

Table 1.1: Core numerical anchors in the present RBFL/RBFS unified candidate.

Quantity	Value
Median all-point A_b from v7 detector	0.552483
Median all-point $A_{\phi,\mathrm{obs}}$	0.558977
Median R_{flat}/R_d	2.522388
Median $A_{\phi,\mathrm{obs}}(R_{\mathrm{flat}})$	0.592761
Median $A_b(R_{\mathrm{flat}})$	0.568646
Median $P_{\mathrm{3D}}(R_{\mathrm{flat}})$	1.064912
Median $Z_{\mathrm{phase}}(R_{\mathrm{flat}})$	0.939044
Median reconstructed h_ϕ/R_d	0.277619
Median integrated projection boost, reconstructed/v7	1.105486
Normal weak-lensing projection band, discovery estimate	1.09–1.18
Fixed v7 group-fold median galaxy APE	13.623%
v9/v18 impedance candidate group-fold median galaxy APE	11.888%

1.3 The discovery path in one diagram

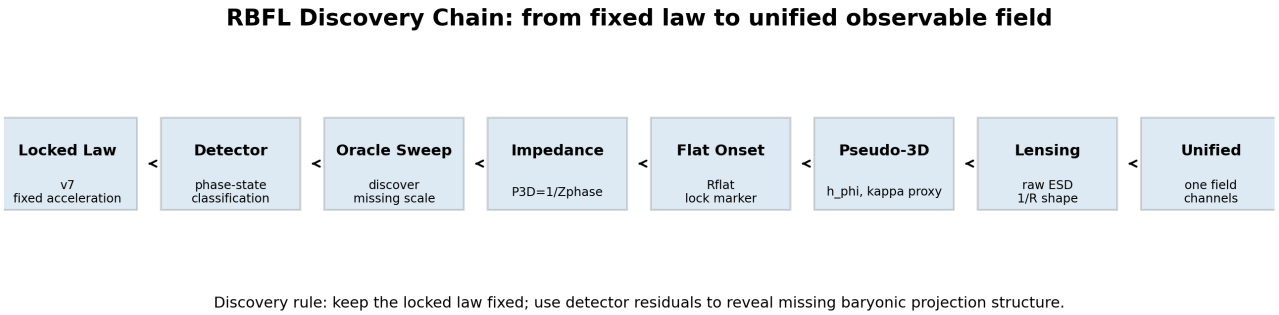

Figure 1.2: The RBFL discovery chain. Each stage was kept as a discovery layer unless and until it could be converted into a fixed baryonic structure rule.

Chapter 2

The starting point: baryons, rotation curves, and the locked law

2.1 Why the original problem was not simply "fit a curve"

Galaxy rotation curves encode a tension between the baryonic matter that is observed and the dynamical support implied by the observed circular velocity. The ordinary radial acceleration inferred from visible baryons is

$$g_b(R) \simeq \frac{GM_b(<R)}{R^2}, \tag{2.1}$$

while the observed acceleration inferred from a circular velocity measurement is

$$g_{\rm obs}(R) = \frac{V_{\rm obs}^2(R)}{R}. \tag{2.2}$$

RBFL began by asking whether the mismatch could be represented as a saturated baryonic response rather than as an arbitrary per-galaxy dark-halo fit. The early radial law took the form

$$g_{\rm RBFL}(R) = g_b(R) + A_\phi(R)\sqrt{a_\phi g_b(R)}. \tag{2.3}$$

This formula already contains a MOND-like low-acceleration square-root structure, so the square-root term alone is not enough to distinguish RBFL from other low-acceleration phenomenologies. The distinctive burden became: can the amplitude A_ϕ, later renamed A_b, be predicted from baryonic structure before residuals are inspected?

2.2 Vector form of the locked law

The radial law was later promoted to a three-dimensional vector expression:

$$\boldsymbol{g}_{\rm RBFL}(\boldsymbol{x},t) = \boldsymbol{g}_b(\boldsymbol{x},t) + A_b(\boldsymbol{x},t)\sqrt{a_\phi|\boldsymbol{g}_b(\boldsymbol{x},t)|}\,\hat{\boldsymbol{g}}_b(\boldsymbol{x},t). \tag{2.4}$$

The law is called *locked* because its structure is not changed every time a detector channel is added. New information can refine the estimate of A_b, but it cannot insert a new acceleration term into Eq. (2.4) without becoming a different theory.

Locked-law rule

A diagnostic channel may help estimate, classify, or falsify A_b. It may not become a hidden acceleration term inside $\boldsymbol{g}_{\rm RBFL}$ unless the theory is explicitly redefined and retested as a new version.

2.3 The outer locked limit and the BTFR-like scaling

In the outer region where the baryonic acceleration is small and the phase operator approaches a locked value,

$$g_b(R) = \frac{GM_b}{R^2}, \qquad A_b(R) \to A_{\rm lock}, \tag{2.5}$$

then the phase-response term dominates over the direct Newtonian term:

$$g_{\rm RBFL}(R) \approx A_{\rm lock}\sqrt{a_\phi \frac{GM_b}{R^2}} \tag{2.6}$$

$$= \frac{A_{\rm lock}\sqrt{GM_b a_\phi}}{R}. \tag{2.7}$$

For a circular orbit, $V_f^2/R = g_{\rm RBFL}$, so

$$V_f^2 \approx A_{\rm lock}\sqrt{GM_b a_\phi}. \tag{2.8}$$

Squaring gives

$$\boxed{V_f^4 \approx GM_b\, a_\Theta}, \qquad \boxed{a_\Theta = A_{\rm lock}^2 a_\phi}. \tag{2.9}$$

This explains why RBFL naturally falls into the same broad low-acceleration scaling family as the baryonic Tully-Fisher relation. It also explains why the novelty cannot be the scaling alone. The novelty must be a baryon-derived rule for A_b.

Chapter 3

The crucial separation: law versus detector

3.1 The phase operator

The v7 architecture separated the acceleration law from the multi-channel Phase Field Prediction/Detection Unit. The baryon-derived phase operator was written as

$$\boxed{A_b(\boldsymbol{x},t) = A_{\rm lock}\, S_{\rm phase}\, D_{\rm phase}\, H_{\rm phase}\, G_{\rm rot}\, B_{\rm switch}} \tag{3.1}$$

where each factor has a different physical or diagnostic role.

Table 3.1: Phase-operator factors in the v7 framework.

Factor	Meaning
$A_{\rm lock}$	Outer locked reference amplitude. In the low-acceleration limit it sets $a_\Theta = A_{\rm lock}^2 a_\phi$.
$S_{\rm phase}$	Phase strength or saturation response. A radial first approximation is $\tanh[(\Sigma_b/\Sigma_c)^p]$.
$D_{\rm phase}$	Coherence/degree factor. Smooth baryonic structure supports coherent phase response; sharp fragmentation or gradients suppress it.
$H_{\rm phase}$	Height/envelope factor. This is the most underdetermined term when only projected/radial data are available.
$G_{\rm rot}$	Rotational organization term. It measures central-node rotation, disk shear, bar/bulge organization, and angular-momentum coherence.
$B_{\rm switch}$	Boundary or switching factor. It marks phase slips, disk-to-HI transitions, and regions where a smooth radial state changes class.

3.2 Prediction side and detection side

The prediction side uses baryonic observables to compute A_b. The detection side reconstructs the phase amplitude implied by the observed rotation curve only after prediction is scored:

$$\boxed{A_{\phi,\rm obs}(R) = \frac{g_{\rm obs}(R) - g_b(R)}{\sqrt{a_\phi g_b(R)}}.} \tag{3.2}$$

The acceleration-ratio detector is

$$\Phi(R) = \frac{g_{\rm obs}(R)}{g_b(R)} = \frac{V_{\rm obs}^2(R)}{V_{\rm bar}^2(R)}, \qquad y(R) = \ln \Phi(R). \tag{3.3}$$

Why residuals must not define the prediction

If $A_{\phi,\mathrm{obs}}$ is used to build A_b in the same step, RBFL becomes a residual-fitting language. If A_b is computed from declared baryonic observables and only then compared to $A_{\phi,\mathrm{obs}}$, RBFL becomes falsifiable.

3.3 The detector states

The detector classified galaxies or radial regions into phase states: weak/void, suppressed, locked, amplified, and switching. These labels were initially diagnostic. They helped determine whether a mismatch was random or structured. They were not allowed to rewrite the law.

The later discovery chain showed that the states were useful but incomplete. State labels alone did not predict the missing local phase amplitude. The missing information was not simply "this galaxy is locked" or "this galaxy is suppressed." It was a continuous projected impedance.

Chapter 4

First sweeps: from tuning instrument to measured target

4.1 Why sweeping was scientifically allowed as discovery

The early detector sweep should be understood like an instrument scan. When a system may contain an unknown response band, one scans to find the response and then asks whether the response can be predicted by physical variables. The scan itself is not the final law.

The discovery-only sweep used a scale s in

$$g_{\mathrm{pred}}(R; s) = g_b(R) + s\, A_b(R)\sqrt{a_\phi g_b(R)}. \tag{4.1}$$

When s was chosen by the data, it was an oracle. When s was replaced by a baryonic rule, it became a closure candidate.

4.2 v0-v3: the first closure attempts

The first sweeps showed that the data contained a powerful missing local response, but a single galaxy-wide scale was too crude. The local radial oracle could nearly remove point-level velocity mismatch, while learned closures from available SPARC variables did not yet generalize strongly.

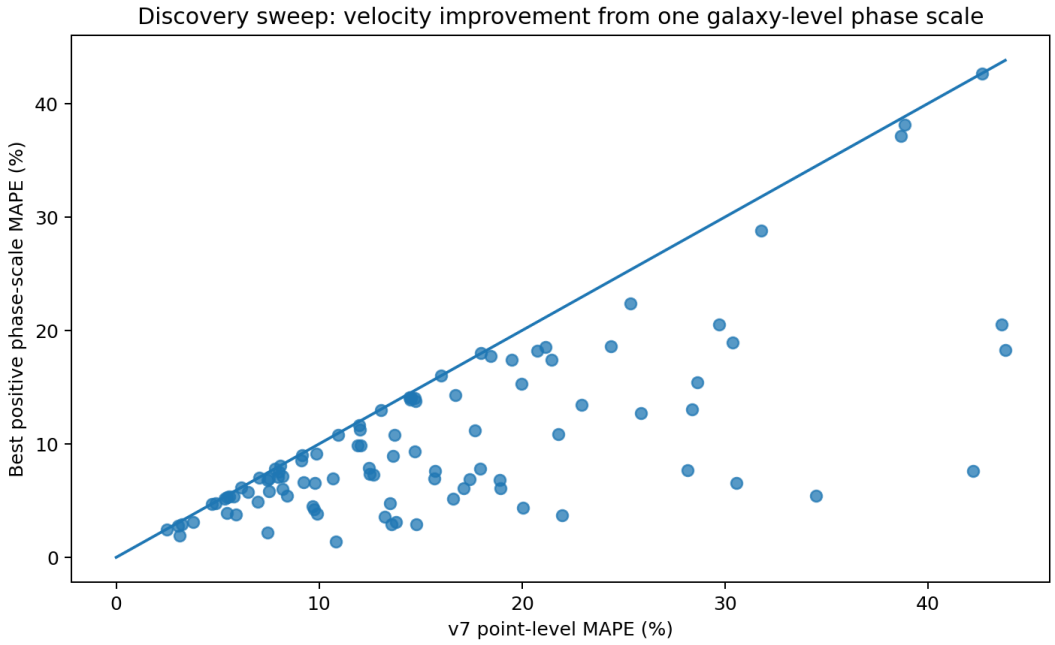

Figure 4.1: The first discovery sweep compared fixed v7 performance against best positive-scale responses. The result showed that the response existed, but the scale itself was still an oracle.

The important lesson was methodological: keep the sweep as a discovery measurement, not as a permanent parameter. The question became

$$s_{\text{best}} \quad \longrightarrow \quad f(\text{baryonic structure}). \tag{4.2}$$

Chapter 5

The missing link: baryonic phase impedance

5.1 v4: the ratio that revealed the hidden object

The first major conceptual breakthrough came when the local sweep scale was reinterpreted as a ratio:

$$\boxed{\lambda_{\text{required}}(R) = \frac{A_{\phi,\text{obs}}(R)}{A_{b,\text{v7}}(R)}.} \tag{5.1}$$

This said that the detector was not simply asking for more or less gravity. It was measuring how the observed phase amplitude compared to the v7 baryon-derived phase operator.

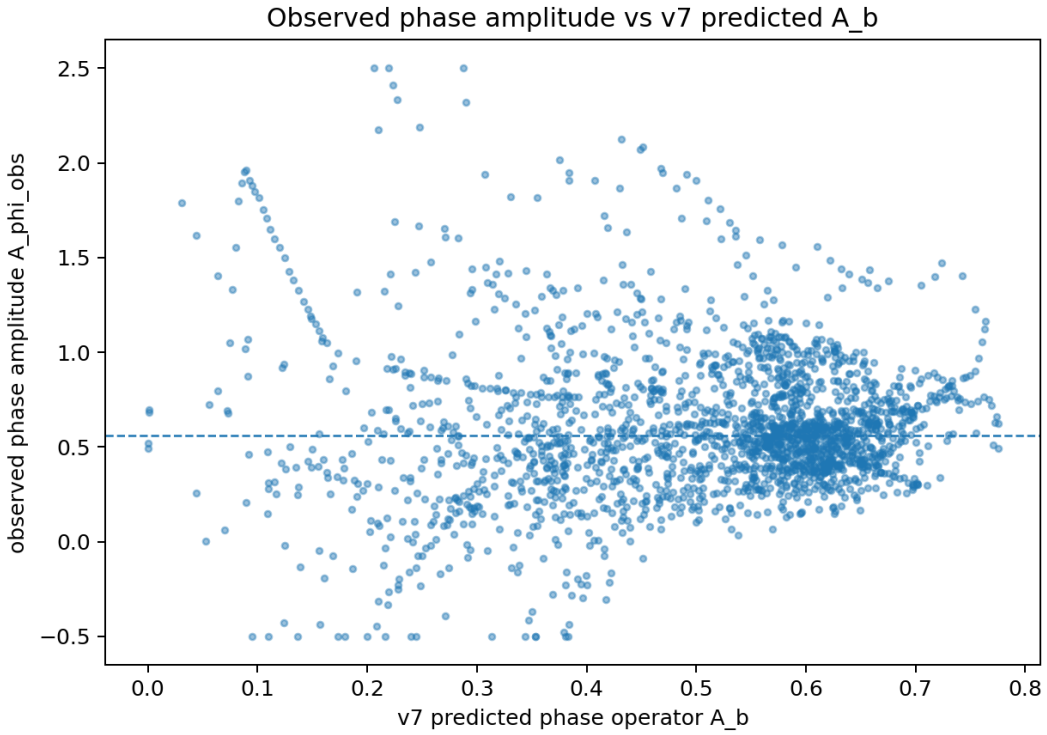

Figure 5.1: v4 compared the observed phase amplitude $A_{\phi,\text{obs}}$ against the v7 predicted operator A_b. The central amplitudes were close, but local projection/impedance mismatches remained.

5.2 v5: defining P_{3D} and Z_{phase}

The ratio was then named as the projected 3D phase correction:

$$\boxed{P_{3D}(R) = \frac{A_{\phi,\mathrm{obs}}(R)}{A_{b,\mathrm{v7}}(R)}} \tag{5.2}$$

with reciprocal phase impedance

$$\boxed{Z_{\mathrm{phase}}(R) = \frac{1}{P_{3D}(R)} = \frac{A_{b,\mathrm{v7}}(R)}{A_{\phi,\mathrm{obs}}(R)}.} \tag{5.3}$$

The interpretation was:

$$P_{3D}(R) \approx \frac{H_{\mathrm{phase,true}}(R, z, \text{line of sight})}{H_{\mathrm{phase,SPARC-proxy}}(R)}. \tag{5.4}$$

SPARC gives a radial/projection shadow. RBFL is trying to infer the 3D envelope that casts that shadow.

Baryonic phase impedance

Z_{phase} is the effective resistance of the baryonic phase carrier to appearing as the local projected response measured by rotation curves. It is not necessarily material resistance; it is a geometric/-transport impedance produced by source coherence, rotation, radial taper, vertical depth, and boundary switching.

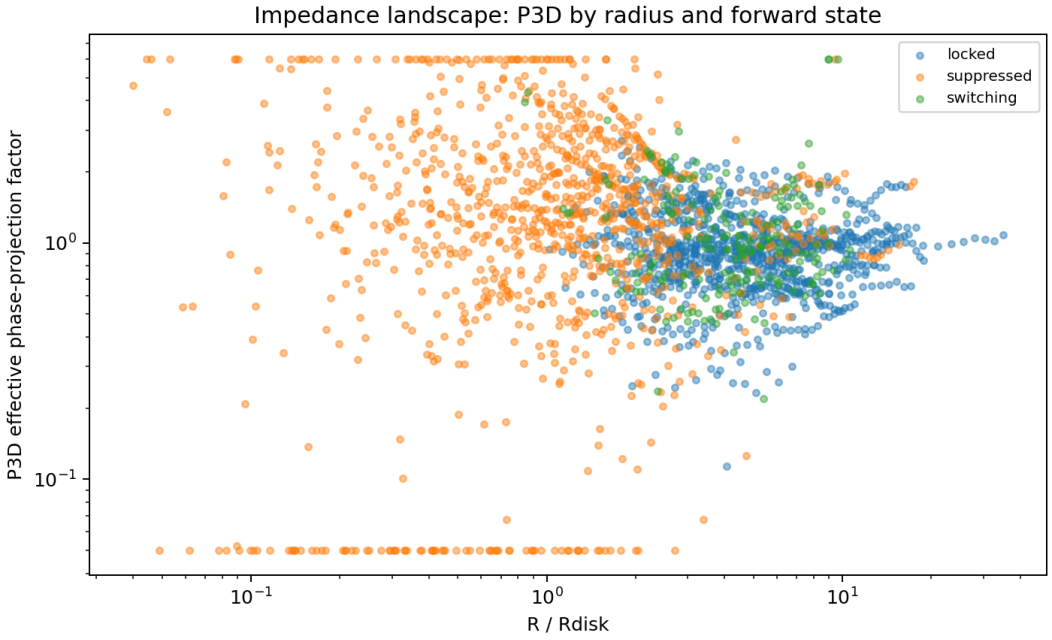

Figure 5.2: v5 mapped P_{3D} across radius and state. The states separated in impedance space, but the missing response remained continuous rather than purely categorical.

Chapter 6

Compressing the sweep into a formula

6.1 v6: multiplicative impedance closure

The next step was to fit P_{3D} as a positive multiplicative quantity. This led to a log-linear bridge:

$$P_{3D}(R) = \exp\left[c_0 + \sum_i c_i z_i(R)\right], \tag{6.1}$$

where z_i were standardized structural variables. This was not yet a physical law, because standardized variables depend on the sample. But it proved that the sweep response was learnable.

The v6 result improved the original holdout median MAPE from roughly 10.29% for fixed v7 to about 7.98% for the best multiplicative closure, while group-fold galaxy testing improved from about 11.90% to about 11.29%. The oracle remained much better, so the formula was a bridge, not the endpoint.

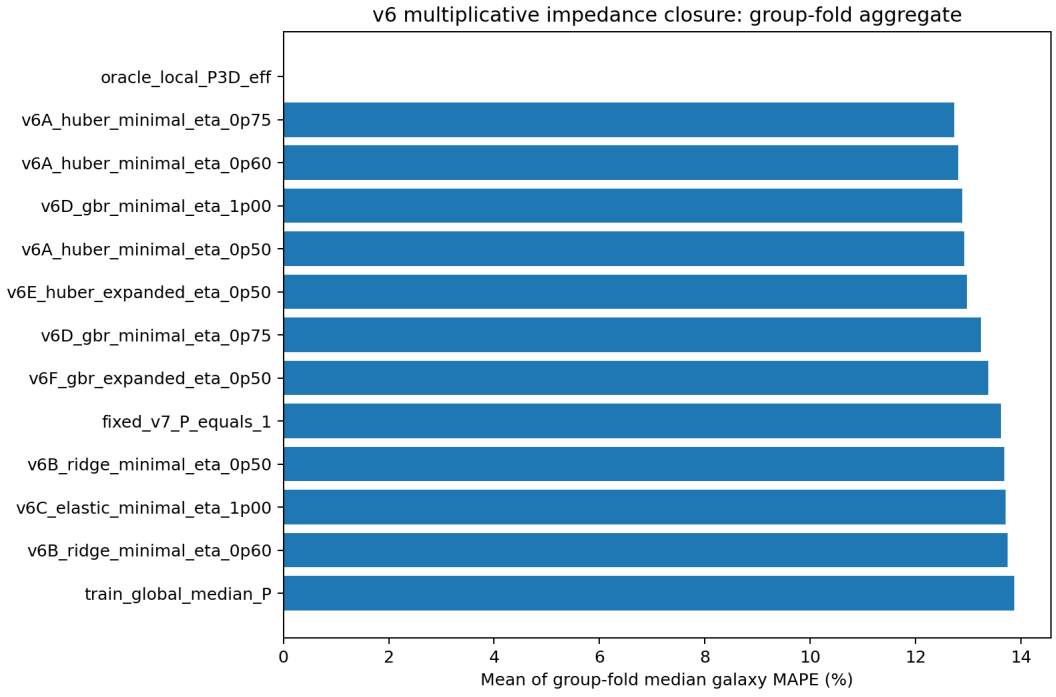

Figure 6.1: v6 group-fold comparison. The multiplicative impedance bridge began to replace the sweep with a learnable baryonic structure rule, but the oracle gap remained.

6.2 v7: replacing z-scores with dimensionless physical ratios

To move from data science back toward physics, the standardized variables were replaced with dimensionless ratios such as

$$\frac{R}{R_d}, \quad \frac{R_{\rm HI}}{R_d}, \quad \frac{g_b}{a_\phi}, \quad \frac{\Sigma_b}{\Sigma_c}, \quad \left|\frac{d\ln\Omega_b}{d\ln R}\right|, \quad \left|\frac{d\ln\Sigma_b}{d\ln R}\right|. \tag{6.2}$$

The transparent linear product helped, but nonlinear physical-ratio benchmarks did better. That showed that the geometry variables were correct but coupled.

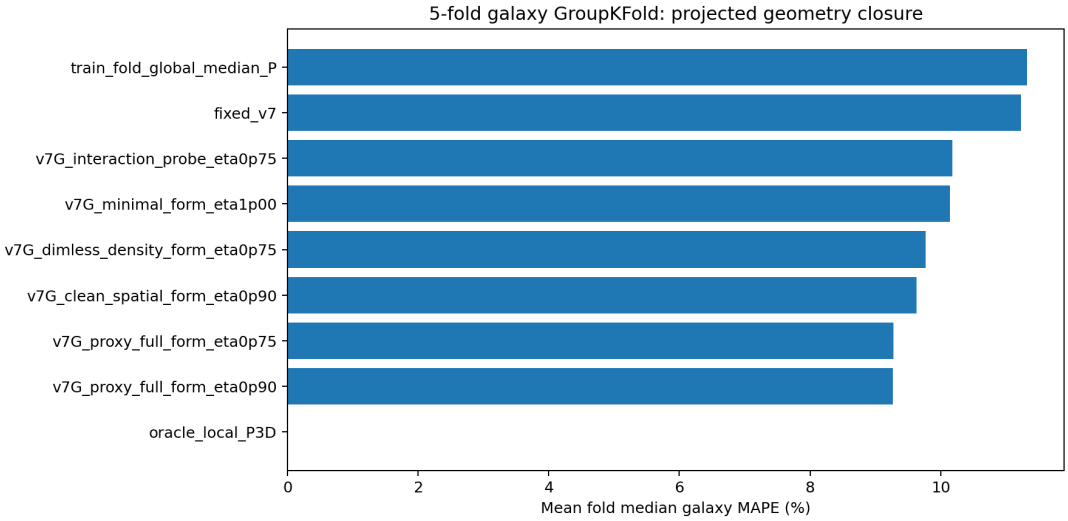

Figure 6.2: v7 projected-geometry closure. Dimensionless physical ratios carried information, but a simple independent product did not fully capture the response.

6.3 v8: coupled form factors

The v8 hypothesis was that geometry enters through products:

$$P_{\rm 3D} = \exp\left[c_0 + aG_{\rm depth} + bG_{\rm rot} + cG_{\rm boundary} + f(G_{\rm depth}G_{\rm radial}) + g(G_{\rm rot}G_{\rm boundary}) + \cdots\right]. \tag{6.3}$$

This is not arbitrary embellishment. In a 3D field envelope, inclination/depth cannot act independently of radius, and rotation cannot act independently of boundary shear. The run confirmed the coupling direction but also showed that too many terms weaken interpretability.

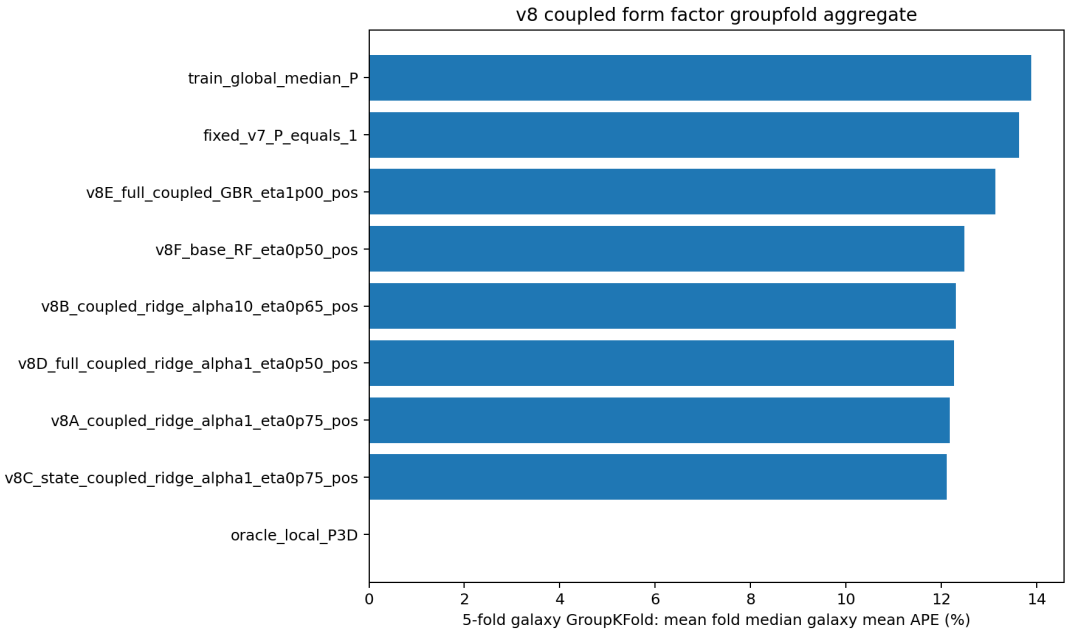

Figure 6.3: v8 showed that coupled projected-geometry terms outperform fixed v7 in group testing, but the formula needed pruning.

6.4 v9: pruned impedance unification

The v9 pruning pass collapsed the broad coupled landscape into a smaller candidate:

Pruned impedance closure

$$P_{\mathrm{3D}}^{\mathrm{pruned}}(R) = \exp\Big[c_0 + c_1 G_{\mathrm{source}} + c_2 G_{\mathrm{depth}} + c_3 G_{\mathrm{boundary}} + c_4 (G_{\mathrm{depth}} G_{\mathrm{radial}}) + c_5 (G_{\mathrm{depth}} G_{\mathrm{boundary}}) + c_6 (G_{\mathrm{source}} \tag{6.4}$$

The v9 read-between-the-lines result was:

$$\text{source coherence} \rightarrow \text{creates the carrier}, \tag{6.5}$$

$$\text{rotation} \rightarrow \text{organizes the carrier}, \tag{6.6}$$

$$\text{radial depth} \rightarrow \text{sets transport path length}, \tag{6.7}$$

$$\text{boundary-depth coupling} \rightarrow \text{controls phase slip}. \tag{6.8}$$

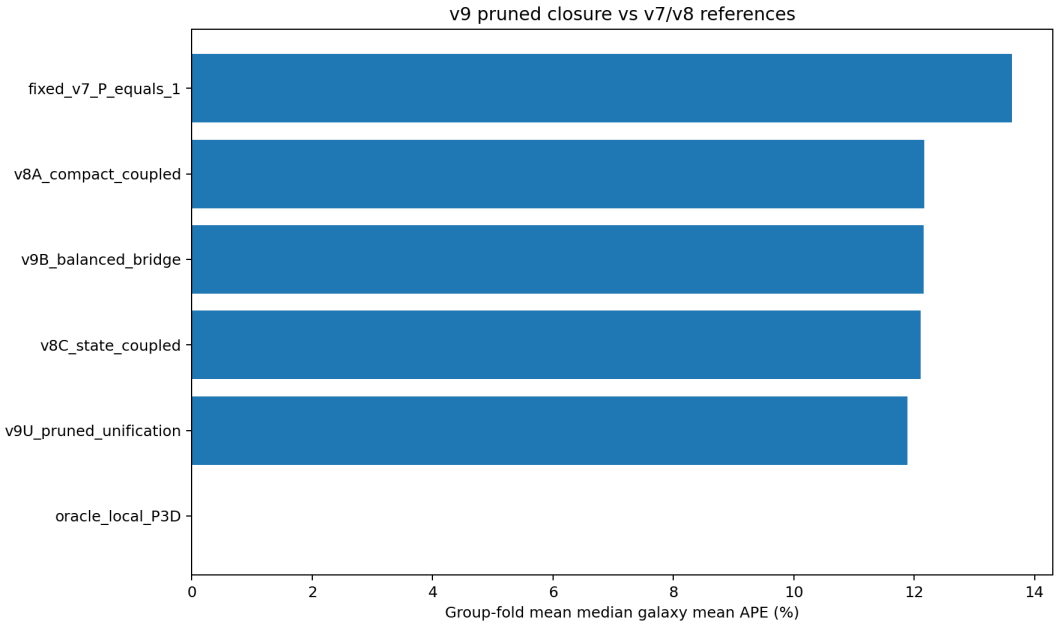

Figure 6.4: v9 pruned closure. The broad impedance landscape reduced to a smaller set of source, depth, radial, rotation, and boundary couplings.

Chapter 7

Flat-onset: where the disk locks

7.1 The stabilization radius

A crucial new clue came from asking where each observed rotation curve first stabilizes into a flat or plateau-like regime. Define the local velocity slope

$$\alpha_V(R) = \frac{d \ln V_{\rm obs}}{d \ln R}. \tag{7.1}$$

The flat-onset radius is the first radius beyond the inner disk where $|\alpha_V|$ becomes small and the outer velocity scatter remains low:

$$\boxed{R_{\rm flat} \approx R_{\rm lock}, \qquad \left| \frac{d \ln V_{\rm obs}}{d \ln R} \right| \to 0.} \tag{7.2}$$

This is discovery-only because it uses $V_{\rm obs}$ to locate the transition. But it reveals a possible phase-lock marker.

The v10 flat-onset probe found, across 99 galaxies,

$$\text{median} \left(\frac{R_{\rm flat}}{R_d} \right) = 2.522, \tag{7.3}$$

with

$$\text{median } A_{\phi,\rm obs}(R_{\rm flat}) = 0.592761, \qquad \text{median } P_{\rm 3D}(R_{\rm flat}) = 1.064912. \tag{7.4}$$

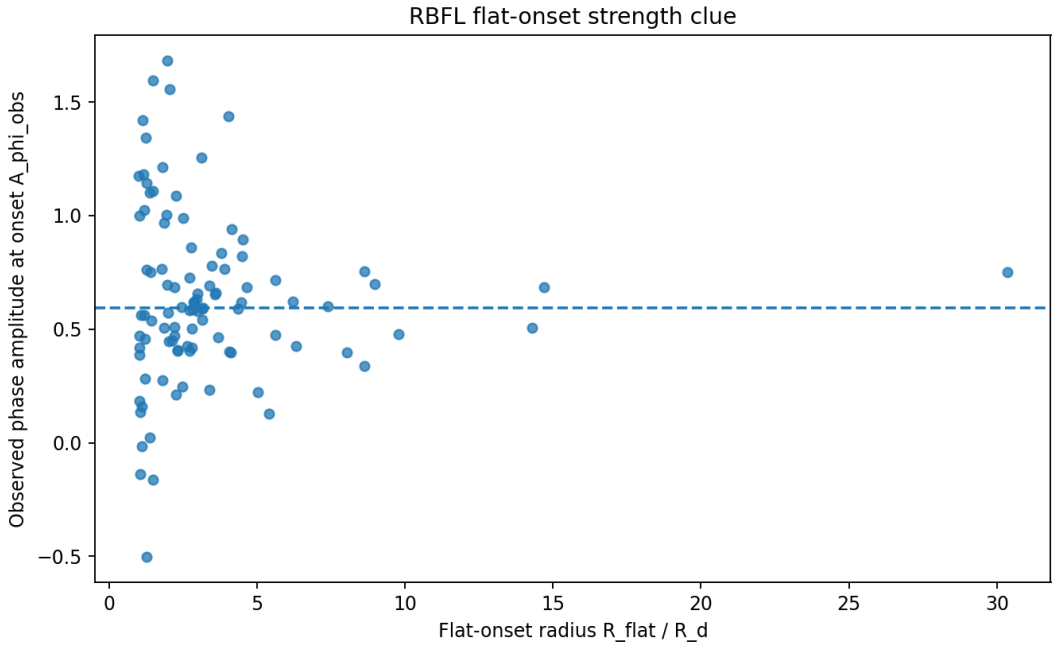

Figure 7.1: v10 flat-onset strength. The onset radius provides a new transition marker where the phase response begins stabilizing into the outer locked regime.

7.2 Why flat onset matters

Before flat onset, the curve is still being shaped strongly by the inner baryonic rise, central concentration, and local disk structure. After flat onset, the system behaves more like a saturated carrier regime. That makes R_{flat} a natural candidate for the transition boundary between inner baryonic response and outer phase lock.

Flat-onset interpretation

The flat-onset radius is not the law. It is a measurable transition marker. If R_{flat} can eventually be predicted from baryonic structure alone, it becomes a powerful closure rule for where the phase field should lock.

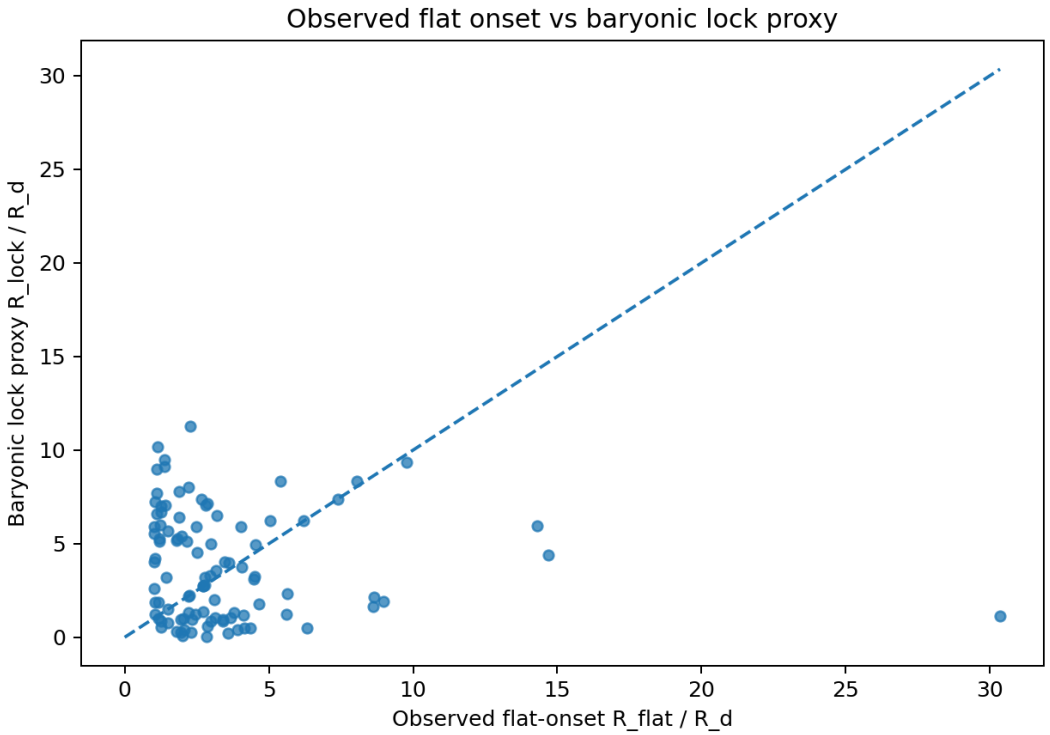

Figure 7.2: v11 compared observed flat onset with baryonic lock proxies. The goal is to replace the observed-onset discovery marker with a predictive baryonic lock radius.

Chapter 8

Pseudo-3D reconstruction

8.1 Why reconstruction is needed

The greatest practical limitation is that SPARC is mostly radial/projected. RBFL is a 3D field model. Without direct $\rho_b(R, \theta, z)$, gas thickness, disk warp, and line-of-sight depth for every galaxy, the detector must infer the missing 3D envelope from radial shadows.

The pseudo-3D reconstruction is therefore not a claim of measured 3D data. It is an inferred field envelope constrained by:

1. the locked law,
2. the phase amplitude $A_{\phi,\mathrm{obs}}$,
3. the impedance $P_{3\mathrm{D}} = 1/Z_{\mathrm{phase}}$,
4. the flat-onset transition R_{flat}, and
5. the gas/radial/rotation/boundary structure available in SPARC-like data.

8.2 Carrier and envelope

The reconstructed carrier is

$$\boxed{A_{\mathrm{carrier}}(R) = A_{b,\mathrm{v7}}(R) P_{3\mathrm{D}}(R).} \tag{8.1}$$

A simple vertical phase envelope was then represented as

$$\boxed{\Phi_{\mathrm{phase}}(R, z) = A_{\mathrm{carrier}}(R)\,\mathrm{sech}^2\left(\frac{z}{h_\phi(R)}\right).} \tag{8.2}$$

For this envelope,

$$\int_{-\infty}^{\infty} \Phi_{\mathrm{phase}}(R, z)\, dz = 2h_\phi(R) A_{\mathrm{carrier}}(R). \tag{8.3}$$

This turns a radial phase reconstruction into a line-of-sight projection target.

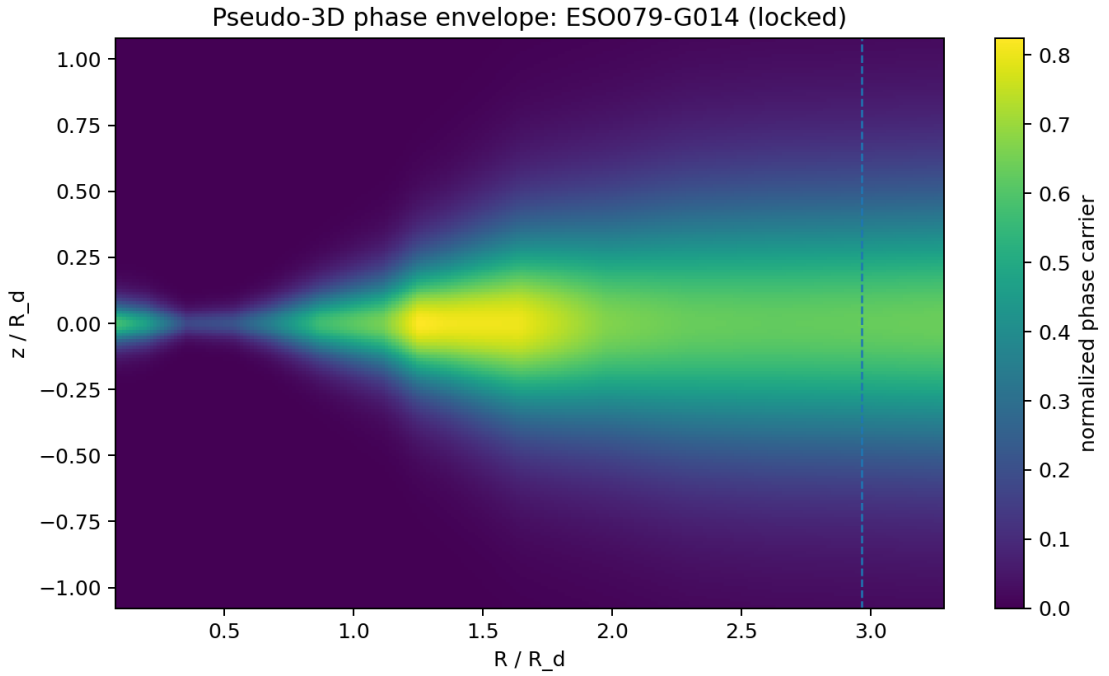

Figure 8.1: Example pseudo-3D R, z phase envelope. This is reconstructed structure, not direct measured 3D baryonic data.

8.3 Projection proxy

The line-of-sight projection proxy is

$$\tilde{\kappa}_\phi(R) \propto 2h_\phi(R)A_{\mathrm{carrier}}(R). \tag{8.4}$$

This is not yet a calibrated lensing convergence. It is the normalized phase-column target that a lensing channel should eventually test.

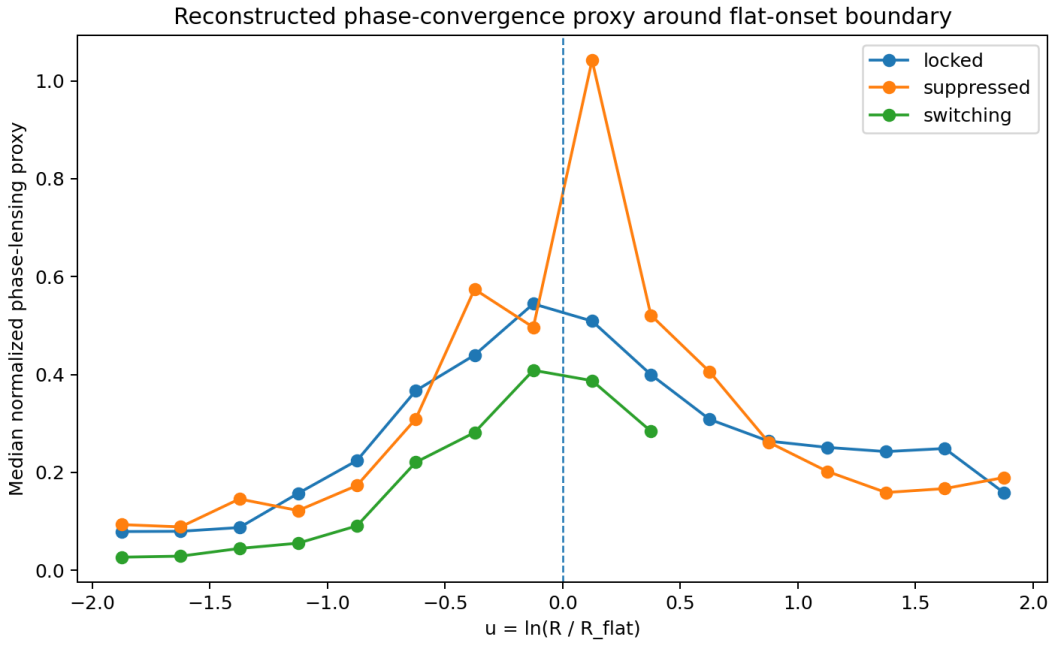

Figure 8.2: v12 normalized phase-lensing projection proxy versus flat-coordinate. This is the first bridge from rotation-derived phase structure to a lensing-style projected observable.

Chapter 9

Lensing bridge: from projected field to raw ESD

9.1 Why lensing is the natural 3D companion

Rotation curves measure local radial acceleration. Weak lensing measures projected line-of-sight response. This makes lensing the natural test of whether P_{3D} truly represents a 3D projection/impedance factor rather than a rotation-curve artifact.

For ordinary galaxy-galaxy lensing, the measured tangential shear is expressed through an excess surface density profile $\Delta\Sigma(R)$. The raw Brouwer/KiDS files used in v16 contain tangential excess surface density and a multiplicative bias correction, so the corrected signal is

$$\boxed{\Delta\Sigma_{\rm corr}(R) = \frac{\mathrm{ESD}_t(R)}{\mathrm{bias}(R)}.} \tag{9.1}$$

For a flat circular-velocity profile,

$$V_c^2(R) \propto R\Delta\Sigma(R). \tag{9.2}$$

If V_c is approximately constant, then

$$\boxed{\Delta\Sigma(R) \propto R^{-1}.} \tag{9.3}$$

9.2 v13-v14: external weak-lensing scale and curve shape

The weak-lensing bridge first compared the phase-carrier scale against published weak-lensing RAR/BTFR summaries. The important ladder was:

$$A_{b,\mathrm{v7}}^{\text{all point}} \sim 0.55, \quad A_{\phi,\mathrm{obs}}(R_{\rm flat}) \sim 0.59, \quad A_{\phi,\mathrm{obs}}^{\text{locked onset}} \sim 0.68, \quad A_{\rm lens} \sim 0.70. \tag{9.4}$$

The lensing-derived scale landed closer to the locked flat-onset carrier than to the all-point median, suggesting that weak lensing samples the large-radius projected locked envelope rather than the inner disk average.

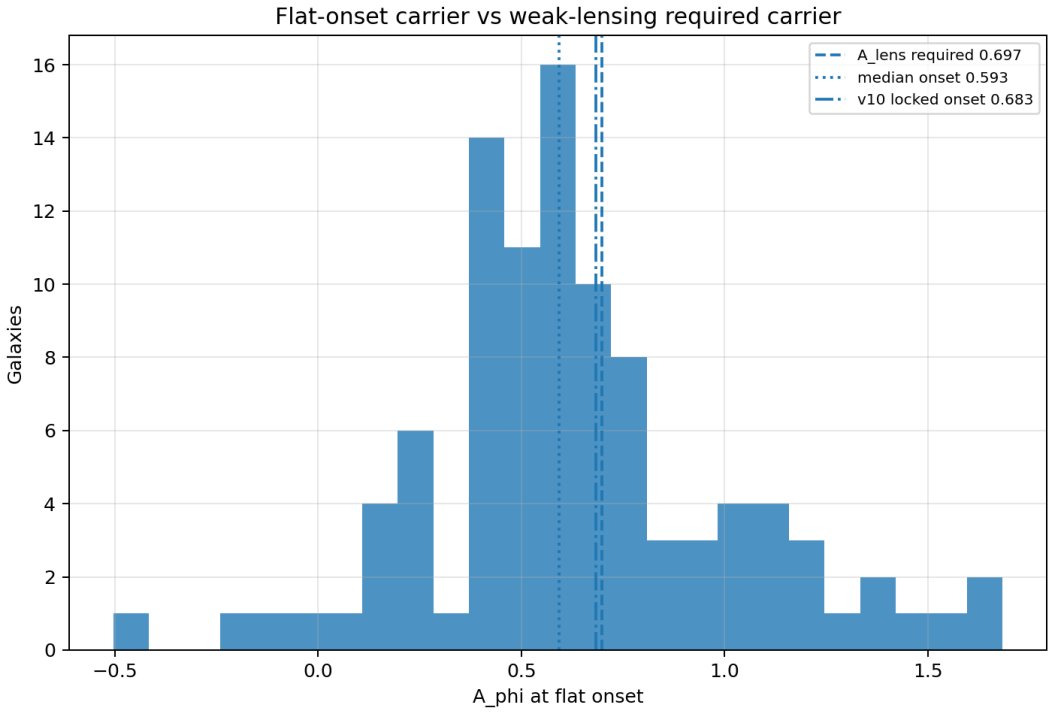

Figure 9.1: v13 carrier comparison. The weak-lensing equivalent carrier lies near the locked flat-onset band rather than the all-point inner/outer average.

The external weak-lensing velocity curves remained very flat out to large radii, consistent with the outer locked-envelope interpretation.

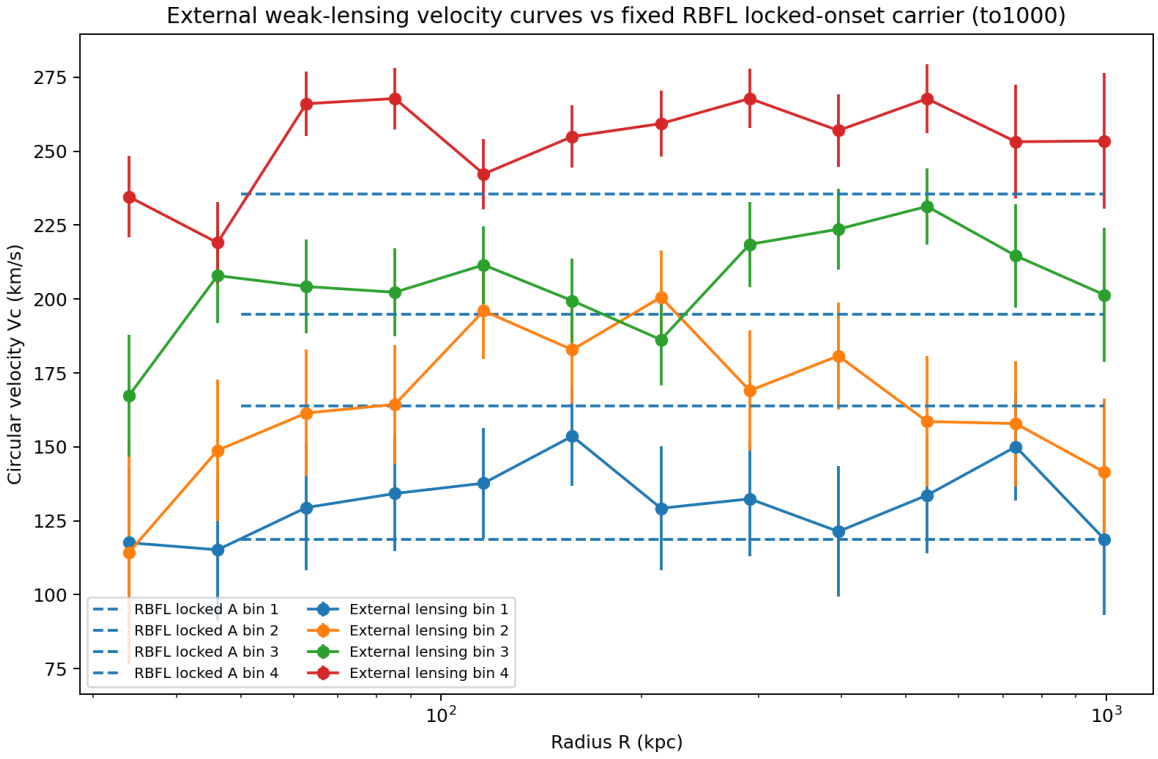

Figure 9.2: v14 weak-lensing velocity curve-shape comparison. The lensing profiles behave like a large-radius flat envelope.

9.3 v16: direct raw ESD shape

The direct raw-ESD ingestion was a major methodological step because it reduced reliance on deprojected circular velocities. The raw corrected ESD profiles themselves showed a close-to-locked-envelope shape:

$$\text{50–300 kpc median ESD log slope} = -0.9294, \tag{9.5}$$

$$\text{50–1000 kpc median ESD log slope} = -0.8994. \tag{9.6}$$

The ideal locked-envelope value is -1. This is not a perfect match, but the profile is close to R^{-1} over the relevant large-radius range.

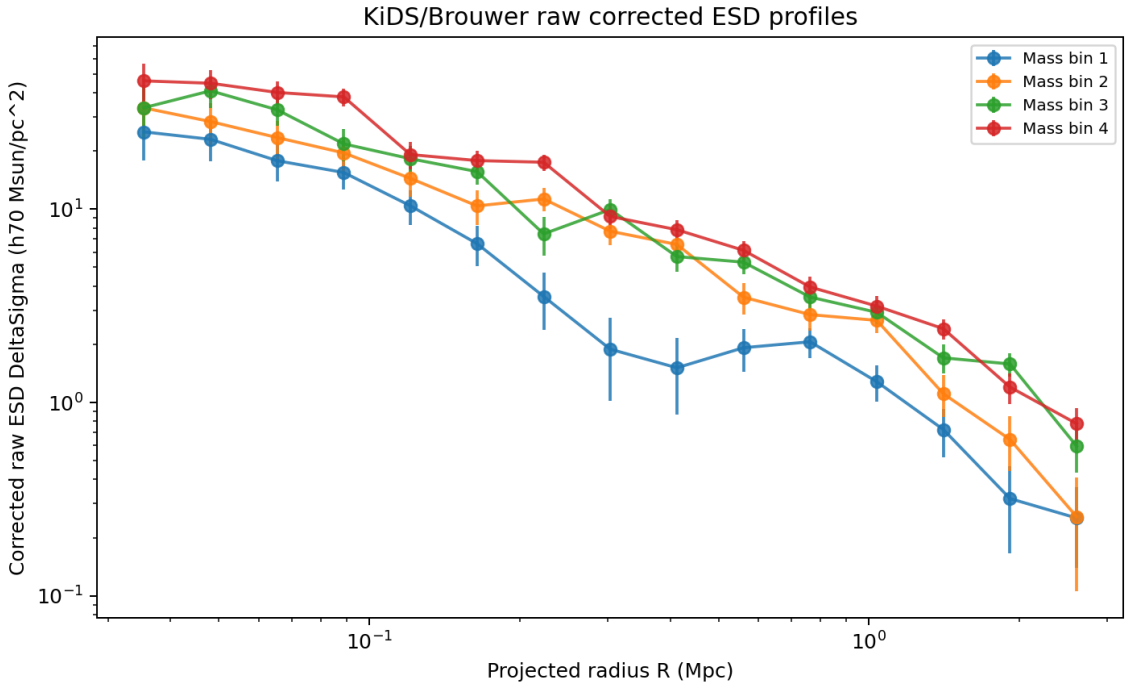

Figure 9.3: v16 direct corrected raw ESD profiles from the Brouwer/KiDS package. The observed profiles are close to the $1/R$ shape expected from a large-radius locked envelope.

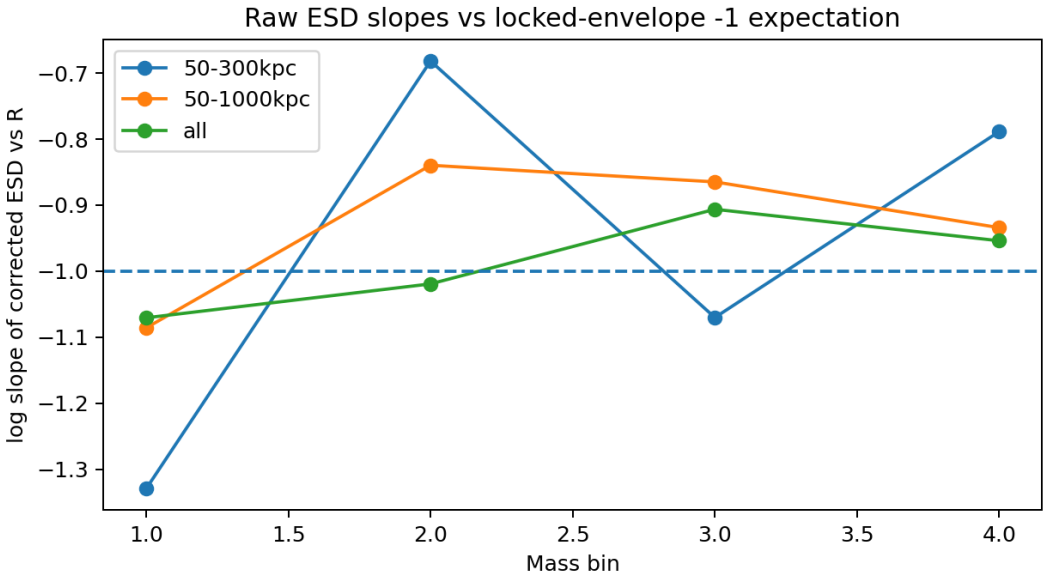

Figure 9.4: v16 ESD slopes compared with the -1 locked-envelope expectation. Shape is stronger than amplitude as the first lensing bridge result.

9.4 v17: the lensing amplitude gap

The raw ESD/RAR acceleration comparison preferred a stronger effective carrier than the SPARC all-point or locked-onset rotation carrier. For the main raw KiDS isolated RAR file,

$$A_{\rm required} \approx 0.8825. \tag{9.7}$$

Relative to the SPARC locked-onset carrier $A_{\rm locked} \approx 0.6831$, this gives

$$\boxed{\Gamma_{\rm lens} = \frac{A_{\rm required}}{A_{\rm locked}} \approx 1.292, \qquad \Gamma^2_{\rm lens} \approx 1.669.} \tag{9.8}$$

Across raw RAR files, the median required carrier was lower, yielding a normal weak-lensing projection band nearer $\Gamma_{\rm lens} \sim 1.09$–$1.18$ for core-to-all categories, with the main isolated file representing a stronger channel.

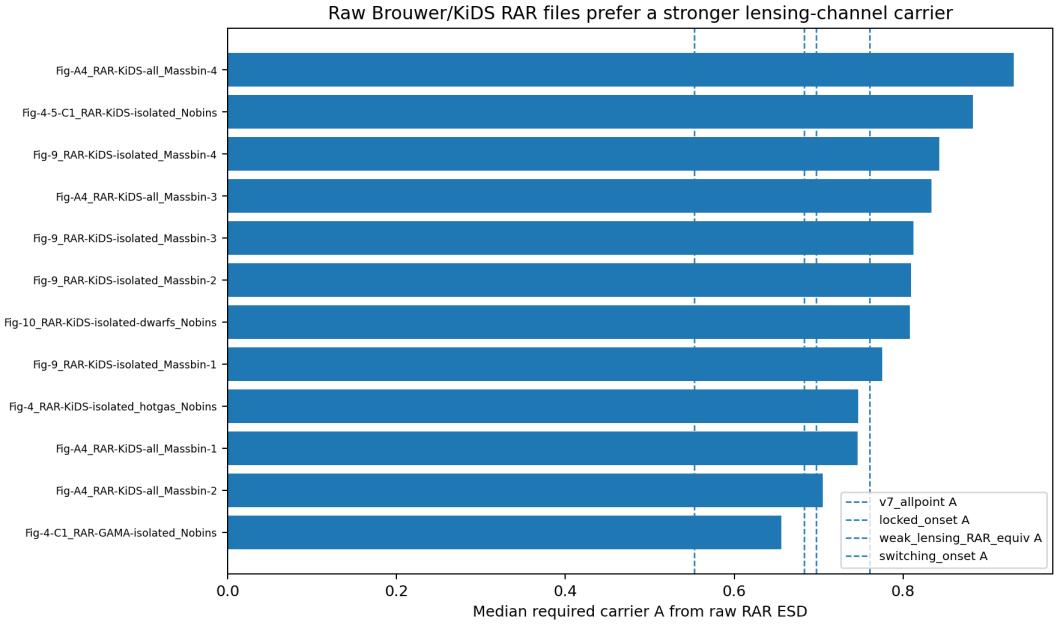

Figure 9.5: v17 required carrier amplitudes by raw RAR file. The amplitude gap is interpreted as a lensing-channel projection normalization, not a change to the acceleration law.

Chapter 10

The unified RBFL/RBFS candidate

10.1 Why unification does not mean one giant fitted formula

A mature theory needs a source equation, a field response, and observable projections. It should not put telescope geometry or line-of-sight integration into the acceleration law itself. The unified RBFL/RBFS candidate therefore keeps the law and observation channels distinct.

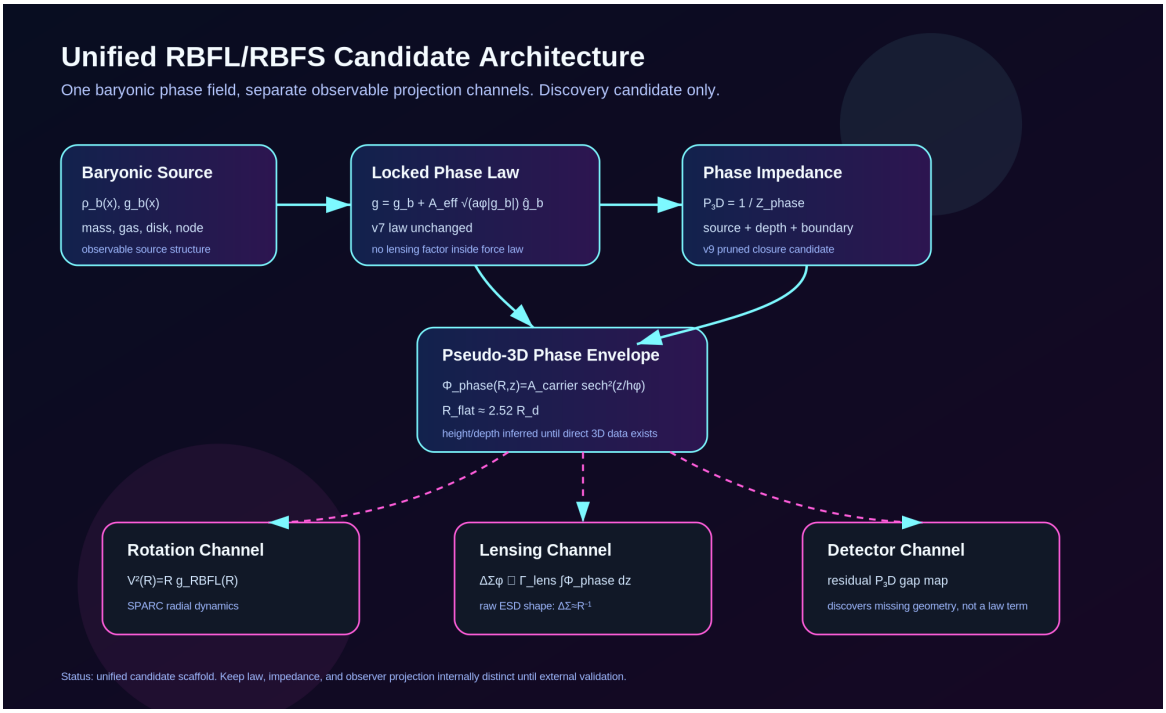

Figure 10.1: v18 unified architecture. One baryon-anchored phase field is mapped into multiple observational channels.

The source field is baryonic:

$$\rho_b(\boldsymbol{x},t) \to \Phi_b(\boldsymbol{x},t) \to \boldsymbol{g}_b(\boldsymbol{x},t). \tag{10.1}$$

The response is phase-amplified:

$$\boldsymbol{g}_\phi(\boldsymbol{x},t) = A_{\rm eff}(\boldsymbol{x},t)\sqrt{a_\phi|\boldsymbol{g}_b(\boldsymbol{x},t)|}\,\hat{\boldsymbol{g}}_b(\boldsymbol{x},t). \tag{10.2}$$

The total acceleration is

$$\boldsymbol{g}_{\rm RBFL} = \boldsymbol{g}_b + \boldsymbol{g}_\phi. \tag{10.3}$$

The phase envelope is reconstructed as

$$\Phi_{\rm phase}(R,z) = A_{\rm carrier}(R)\,\mathrm{sech}^2(z/h_\phi). \tag{10.4}$$

The rotation channel reads the local radial field. The lensing channel reads the line-of-sight integral.

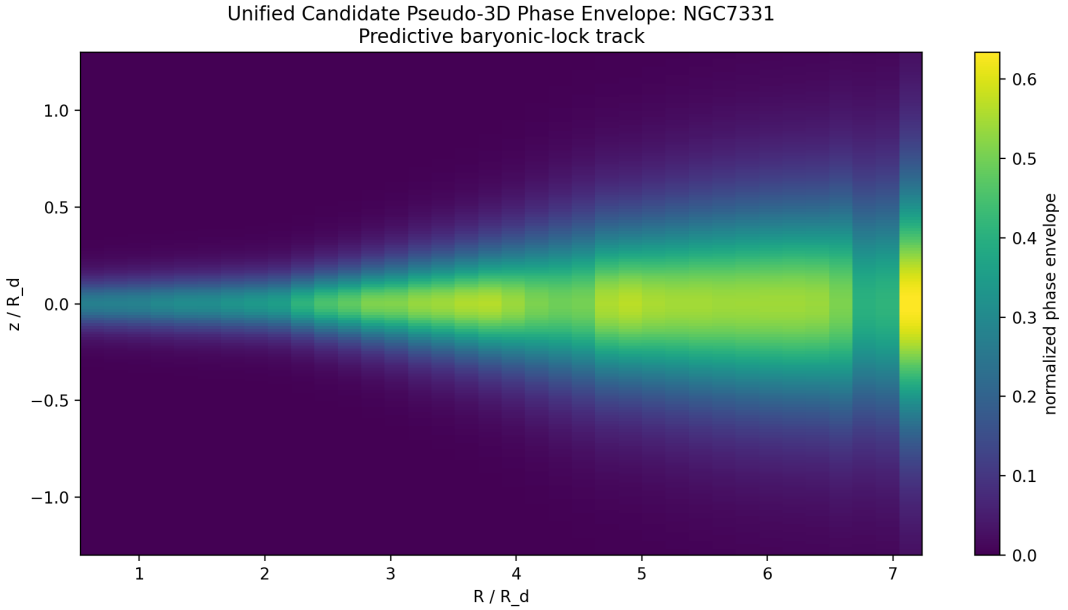

Figure 10.2: v18 NGC7331 pseudo-3D phase envelope demonstration. This visualizes the unified candidate as a field geometry rather than a residual-fitting layer.

10.2 Observable maps

The rotation map is

$$\mathcal{O}_{\mathrm{rot}}[\boldsymbol{g}_{\mathrm{RBFL}}](R) = V(R) = \sqrt{R\, g_{\mathrm{RBFL}}(R)}. \tag{10.5}$$

The lensing map is

$$\mathcal{O}_{\mathrm{lens}}[\Phi_{\mathrm{phase}}](R) = \Gamma_{\mathrm{lens}} \int \Phi_{\mathrm{phase}}(R, z)\, dz. \tag{10.6}$$

The detector residual map is

$$\mathcal{O}_{\mathrm{det}}(R) = \Delta P_{\mathrm{3D}}(R) = P_{\mathrm{3D}}^{\mathrm{oracle}}(R) - P_{\mathrm{3D}}^{\mathrm{pred}}(R). \tag{10.7}$$

The detector remains useful because it tells us what the fixed closure is still missing. It is no longer the theory.

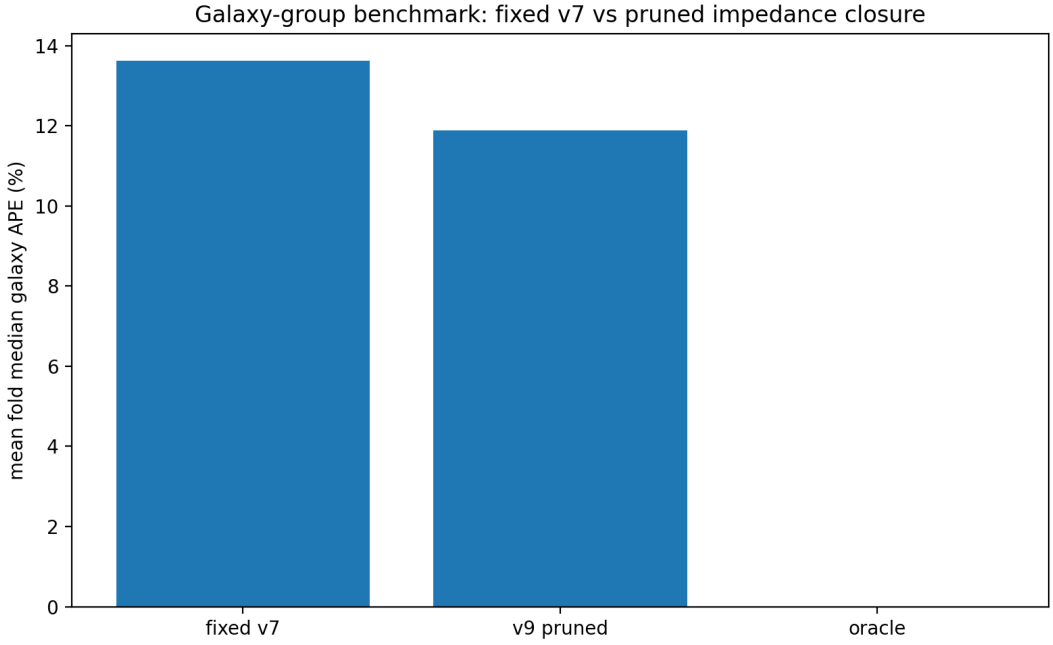

Figure 10.3: v18 benchmark summary. The unified impedance candidate improves over fixed v7 in grouped tests, but it remains far from the oracle, so it is a bridge rather than a final proof.

Chapter 11

Full discovery ledger

Table 11.1: RBFL/RBFS discovery ledger from initial fixed-law detector work to unified candidate.

Stage	Question	Key move	Main lesson
v7 core	Can the law remain fixed?	Locked the acceleration expression $g_b + A_b\sqrt{a_\phi g_b}$.	The law and detector must be separated.
v0	Does a phase-scale sweep improve fits?	Scanned positive scale multipliers.	Sweep finds a response, but a sweep is not a law.
v1	Can a galaxy-wide scale be predicted?	Learned galaxy-level closure.	Too crude; did not robustly beat fixed v7.
v2	Is the missing scale local in radius?	Radial oracle closure.	Local oracle nearly eliminates mismatch, proving the target is local.
v3	Do phase states explain the scale?	State-conditioned models.	State labels help, but are not enough.
v4	What is the hidden measured object?	Defined $A_{\phi,\mathrm{obs}}/A_b$.	Missing term is a phase-amplitude ratio.
v5	What is the physical interpretation?	Named $P_{\mathrm{3D}} = 1/Z_{\mathrm{phase}}$.	The sweep maps baryonic phase impedance/projection.
v6	Can impedance be learned multiplicatively?	$P_{\mathrm{3D}} = \exp(c_0 + \sum c_i z_i)$.	Learnable bridge; not final physics due to z-score dependence.
v7 geometry	Can physical ratios replace z-scores?	Used dimensionless geometry variables.	Ingredients are physical but coupled.
v8	Are there geometry couplings?	Added depth/radial and rotation/boundary products.	Coupling helps; pruning needed.
v9	What is the smallest stable closure?	Pruned to source, depth, boundary, and couplings.	First compact unification candidate.
v10	Where does the disk lock?	Detected flat-onset radius R_{flat}.	$R_{\mathrm{flat}}/R_d \approx 2.52$ marks phase-lock transition.
v11	Can onset become predictive?	Integrated flat-onset with baryonic lock proxies.	Need predict R_{flat} from baryons alone.
v12	Can rotation imply a pseudo-3D envelope?	Built $\Phi(R,z) = A\,\mathrm{sech}^2(z/h)$.	Generated a lensing-style projection target.
v13	Does weak lensing prefer similar carrier scale?	Compared to weak-lensing RAR/BTFR scale.	Lensing scale lies near locked onset.
v14	Does weak lensing show the same outer shape?	Compared external lensing velocity curves.	Large-radius weak-lensing curves are very flat.
v15	What is the ESD-equivalent shape?	Converted lensing velocity to $\Delta\Sigma$-like profiles.	Flat envelope implies $\Delta\Sigma \sim 1/R$.
v16	Does raw ESD itself show this?	Ingested raw Brouwer/KiDS ESD profiles.	Corrected ESD is close to R^{-1}.
v17	Why is lensing amplitude stronger?	Measured $\Gamma_{\mathrm{lens}} = A_{\mathrm{req}}/A_{\mathrm{locked}}$.	Normal weak lensing has a projection-amplification band.
v18	How do all parts unify?	Built one field with separate observable maps.	Unified candidate: law + phase operator + impedance + projection.

Chapter 12

Definitions and symbol dictionary

Table 12.1: Core symbols.

Symbol	Definition
$\rho_b(\boldsymbol{x}, t)$	3D baryonic density: stars, gas, dust, bulge, disk, and compact baryonic structure.
Φ_b	Baryonic gravitational potential satisfying $\nabla^2\Phi_b = 4\pi G\rho_b$.
$\boldsymbol{g}_b$	Baryonic acceleration field, $-\nabla\Phi_b$.
a_ϕ	Phase-carrier acceleration scale.
$\boldsymbol{g}_{\mathrm{RBFL}}$	Total RBFL acceleration field.
A_b	Baryon-derived phase response operator used in the law.
$A_{\phi,\mathrm{obs}}$	Observed residual-derived phase amplitude, calculated after prediction.
A_{lock}	Locked outer-regime phase amplitude.
a_Θ	Locked outer acceleration scale, $a_\Theta = A_{\mathrm{lock}}^2 a_\phi$.
S_{phase}	Strength/saturation factor.
D_{phase}	Coherence/degree factor.
H_{phase}	True 3D height/envelope factor.
H_{proxy}	Projected estimate of the height/envelope available from SPARC-like data.
G_{rot}	Rotational organization/shear factor.
B_{switch}	Boundary switching/slip factor.
P_{3D}	Projected 3D phase correction, $A_{\phi,\mathrm{obs}}/A_b$.
Z_{phase}	Baryonic phase impedance, $1/P_{\mathrm{3D}}$.
R_{flat}	Observed flat-onset radius where $\lvert d\ln V/d\ln R\rvert \to 0$.
R_{lock}	Predicted or interpreted phase-lock radius.
h_ϕ	Reconstructed phase-envelope height scale.
$\Phi_{\mathrm{phase}}(R, z)$	Pseudo-3D phase envelope.
$\Delta\Sigma$	Excess surface density in weak-lensing notation.
Γ_{lens}	Lensing-channel projection amplification factor; not a force-law term.

Chapter 13

What has been learned and what remains open

13.1 The strong results

1. The central phase amplitude is not random. Median $A_{\phi,\mathrm{obs}}$ and median v7 A_b are close at the all-point level.
2. The local oracle response is powerful, meaning the missing term is structured rather than pure noise.
3. The missing response is better understood as $P_{3\mathrm{D}} = 1/Z_{\mathrm{phase}}$, a projected 3D phase-impedance correction.
4. Flat-onset appears to mark a meaningful phase-lock transition near $R_{\mathrm{flat}}/R_d \approx 2.52$.
5. Pseudo-3D reconstruction gives a bridge from rotation curves to a lensing-style line-of-sight projection target.
6. Raw corrected weak-lensing ESD profiles are close to $\Delta\Sigma \sim R^{-1}$, the expected shape for a flat outer locked envelope.

13.2 The unsolved problems

1. $P_{3\mathrm{D}}$ is only partially predicted by the pruned closure. The oracle gap remains.
2. R_{flat} is presently detected from V_{obs}, not predicted blindly from baryons.
3. Full 3D baryonic data are missing for most SPARC galaxies.
4. The lensing projection amplitude Γ_{lens} is not yet predicted from 3D structure.
5. No relativistic action, lensing metric, conservation-law derivation, or cosmological model is yet complete.

13.3 Falsifiability targets

The current candidate becomes stronger only if it survives tests that are not used to discover it. The most important are:

1. freeze the v9/v18 impedance closure and test it on new galaxies;
2. predict R_{flat} from baryonic observables before looking at V_{obs};
3. compare the predicted $P_{3\mathrm{D}}$ residuals against true disk thickness, warp, and gas-envelope data;

4. predict raw $\Delta\Sigma(R)$ amplitude and shape by lensing sample category without refitting $\Gamma_{\rm lens}$;
5. benchmark against MOND/RAR and halo models using identical inputs, identical holdouts, and identical scoring.

The safest public claim

RBFL/RBFS is a speculative, baryon-derived, phase-field research programme. It has produced a reproducible discovery chain in which residual phase structure is increasingly compressed into baryonic impedance and projection terms. It remains unproven until the closure is frozen and externally validated.

Chapter 14

Unified law statement

The present unified law candidate can be stated as follows.

RBFL Unified Law Candidate

$$\boldsymbol{g}_{\mathrm{RBFL}}(\boldsymbol{x},t) = \boldsymbol{g}_b(\boldsymbol{x},t) + \boldsymbol{g}_\phi(\boldsymbol{x},t), \tag{14.1}$$

$$\boldsymbol{g}_\phi(\boldsymbol{x},t) = A_{\mathrm{eff}}(\boldsymbol{x},t)\sqrt{a_\phi|\boldsymbol{g}_b(\boldsymbol{x},t)|}\,\hat{\boldsymbol{g}}_b(\boldsymbol{x},t), \tag{14.2}$$

$$A_{\mathrm{eff}}(\boldsymbol{x},t) = A_{\mathrm{lock}} S_{\mathrm{phase}} D_{\mathrm{phase}} G_{\mathrm{rot}} B_{\mathrm{switch}} H_{\mathrm{proxy}} P_{\mathrm{3D}}, \tag{14.3}$$

$$P_{\mathrm{3D}}(\boldsymbol{x},t) = Z^{-1}_{\mathrm{phase}}(\boldsymbol{x},t), \tag{14.4}$$

$$Z^{-1}_{\mathrm{phase}}(R) \approx \exp\Big[c_0 + c_1 G_{\mathrm{source}} + c_2 G_{\mathrm{depth}} + c_3 G_{\mathrm{boundary}} + c_4 G_{\mathrm{depth}} G_{\mathrm{radial}} + c_5 G_{\mathrm{depth}} G_{\mathrm{boundary}} + c_6 G_{\mathrm{source}} G_{\mathrm{rotation}}\Big]. \tag{14.5}$$

For rotation curves:

$$V^2(R) = R\,\hat{\boldsymbol{R}} \cdot \boldsymbol{g}_{\mathrm{RBFL}}(R). \tag{14.6}$$

For lensing-style projection:

$$\Delta\Sigma_\phi(R) \propto \Gamma_{\mathrm{lens}} \int \Phi_{\mathrm{phase}}(R,z)\,dz, \qquad \Phi_{\mathrm{phase}} = A_{\mathrm{carrier}}\,\mathrm{sech}^2(z/h_\phi). \tag{14.7}$$

The same field, not separate laws, produces both observable channels.

Source and reproducibility notes

This PDF synthesizes the uploaded RBFL materials and the generated discovery packages through v18. The main internal source artifacts are:

- `RBFL_Full_Reproducibility_Package_2026_06_13.zip`
- `Breakdown Report on the Current RBFL Position.pdf`
- `RBFL_Gravity_Field_Law_and_Hypothetical_Engineering.pdf`
- `RBFL_Phase_Discovery_Sweep_v0.zip` through `v18`
- `brouwer2021_rar.tar`, the uploaded Brouwer/KiDS ESD package used in the direct raw ESD bridge

The report intentionally keeps discovery results separate from locked-law claims. Any numerical value reported here should be read as a discovery-chain output unless explicitly identified as a fixed theory parameter.

Recommended next frozen tests

1. **Frozen SPARC closure test:** run fixed v7, v9, and v18 formulas on the same full SPARC galaxy list, with no per-galaxy refitting.
2. **Blind onset prediction:** train or derive $R_{\rm lock}/R_d$ from baryonic data only; then compare to observed $R_{\rm flat}/R_d$.
3. **3D data substitution:** replace $H_{\rm proxy}$ with measured disk thickness, HI warp, or line-of-sight gas depth where available.
4. **Raw ESD amplitude test:** predict $\Delta\Sigma(R)$ normalization for each weak-lensing sample category using fixed $\Gamma_{\rm lens}$ bands.
5. **External benchmark:** compare against MOND/RAR and NFW/Burkert halo baselines under identical holdout partitions.

Closing statement

The RBFL journey began with a simple baryon-derived square-root acceleration law. That law alone was not enough; it belonged to a known low-acceleration scaling family. The scientific work began when the framework separated the law from the detector and asked whether the phase amplitude could be predicted from baryonic structure.

The detector sweeps then revealed a hidden local ratio. That ratio became P_{3D}. Its reciprocal became Z_{phase}, baryonic phase impedance. Flat-onset analysis revealed where the disk appears to lock into the saturated carrier regime. Pseudo-3D reconstruction turned radial phase strength into an inferred field envelope. Weak-lensing and raw ESD bridges then showed that the large-radius projected field has the expected locked-envelope shape.

The unified candidate is therefore not a claim that the problem is solved. It is the first coherent architecture in which the pieces fit:

$$\text{baryons} \rightarrow \text{phase operator} \rightarrow \text{phase impedance} \rightarrow \text{3D envelope} \rightarrow \text{rotation and lensing observables.} \tag{14.8}$$

That is the current RBFL Unified Law candidate.